Non-destructive monitoring of microalgae biofilms

David Morgado, Andrea Fanesi, Thierry Martin, Sihem Tebbani, Olivier Bernard, Filipa Lopes

Bioresource Technology 398 (2024) 130520

Contents lists available at ScienceDirect

Bioresource Technology

journal homepage: www.elsevier.com/locate/biortech

Non-destructive monitoring of microalgae biofilms

David Morgado [a], Andrea Fanesi [a,*], Thierry Martin [a], Sihem Tebbani [b], Olivier Bernard [c], Filipa Lopes [a]

[a] Université Paris-Saclay, CentraleSupélec, Laboratoire Génie des Procédés et Matériaux (LGPM), Gif-sur-Yvette, France
[b] Université Paris-Saclay, CentraleSupélec, CNRS, Laboratoire des Signaux et Systèmes (L2S), Gif sur Yvette, France
[c] INRIA, Centre d'Université Côte d'Azur, Biocore, Sorbonne Université, CNRS, Sophia-Antipolis, France

HIGHLIGHTS

- Proposed a protocol to fill the gap in the monitoring of microalgae biofilm systems.
- Used reflectance spectroscopy to non-destructively quantify biofilm traits.
- Identified reflectance indices that accurately tracked biofilm trait dynamics.
- Robust prediction of astaxanthin under different light and nutrient conditions.

GRAPHICAL ABSTRACT

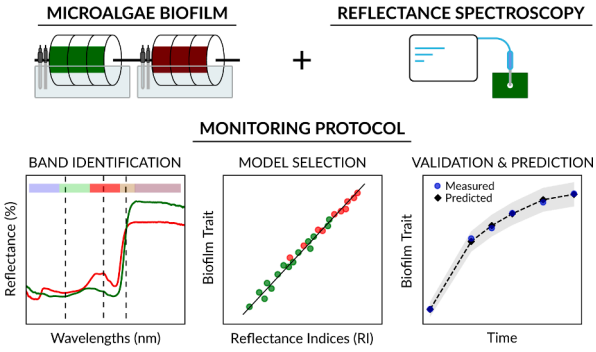

ARTICLE INFO

Keywords:
Astaxanthin
Haeamatococcus pluvialis
Rotating Biofilm
Reflectance Indices
Spectroscopy

ABSTRACT

Biofilm-based cultivation systems are emerging as a promising technology for microalgae production. However, efficient and non-invasive monitoring routines are still lacking. Here, a protocol to monitor microalgae biofilms based on reflectance indices (RIs) is proposed. This framework was developed using a rotating biofilm system for astaxanthin production by cultivating *Haematococcus pluvialis* on cotton carriers. Biofilm traits such as biomass, astaxanthin, and chlorophyll were characterized under different light and nutrient regimes. Reflectance spectra were collected to identify the spectral bands and the RIs that correlated the most with those biofilm traits. Robust linear models built on more than 170 spectra were selected and validated on an independent dataset. Astaxanthin content could be precisely predicted over a dynamic range from 0 to 4% of dry weight, regardless of the cultivation conditions. This study demonstrates the strength of reflectance spectroscopy as a non-invasive tool to improve the operational efficiency of microalgae biofilm-based technology.

1. Introduction

Microalgae are a versatile source of high-value compounds for various markets seeking interest in renewable resources and green economy. Compared to terrestrial plants they exhibit higher growth rates and can thrive in challenging geographic areas that would

* Corresponding author.
E-mail address: andrea.fanesi@centralesupelec.fr (A. Fanesi).

https://doi.org/10.1016/j.biortech.2024.130520
Received 5 January 2024; Received in revised form 26 February 2024; Accepted 29 February 2024
Available online 1 March 2024

otherwise be unfavorable for traditional crops (Moody et al., 2014). However, despite its potential, microalgae farming at an industrial scale remains a small niche in the market economy, primarily due to the high energetic costs associated with both upstream (e.g. cultivation) and downstream processes (Barkia et al., 2019). To tackle this limitation, significant research efforts have been directed towards improving cultivation systems (Assunção & Malcata, 2020) and developing a biorefinery approach for biomass valorization (Slegers et al., 2020).

Concerning the cultivation systems, two distinct technologies can be distinguished. While the classical photobioreactors (PBRs) and raceways have been long established, where microalgae grow suspended in a liquid medium (i.e., planktonic state), a more recent advancement has been the development of biofilm-based technologies. This new approach exploits the microalgae's ability to develop biofilms, allowing them to grow attached to a substrate (Moreno Osorio et al., 2021). By using lower medium volumes and by simplifying harvesting, biofilm-based technologies enable higher biomass yields, resulting in a more energy and cost-efficient process (Morales et al., 2020; Podola et al., 2017)

Regardless of the cultivation technology, efficient monitoring of microalgae culture conditions is of paramount importance. Particularly, the monitoring of biological features (e.g. biomass and cell traits) is the most challenging due to the absence of easy-to-use on-line/in-line systems (Havlik et al., 2022). Monitoring is currently carried out destructively by taking samples off-line, which can be time-consuming, can lead to contaminations, and is unsuitable for continuous monitoring or direct process control (Sá et al., 2022). To address these limitations, recent technological advancements have enabled the integration of optical methods for *in situ* monitoring. Techniques such as UV–Vis, fluorescence and vibrational (FTIR and Raman) spectroscopy provide accurate and rapid detection for monitoring biomass and cellular compounds in classical PBRs (Lieutaud et al., 2019; Liu et al., 2021).

However, with the emergence of biofilm-based systems, novel non-invasive monitoring tools for microalgal biofilms need to be developed. Due to the non-transparent nature of the carrier utilized in biofilm-based systems (i.e. textile fabrics; Mantzorou & Ververidis, 2019), reflectance-based techniques would be preferred over transmission-based configurations. In this context, remote sensing technology, established since decades in precision agriculture (Walsh et al., 2020), could be adapted to microalgae biofilm farming. Historically, remote sensing has been successfully used to monitor phytoplankton in oceans (Blondeau-Patissier et al., 2014), and to characterize natural biofilm communities such as microphytobenthos (MPB) (Méléder et al., 2020). From a commercial point of view, this sensing technology has proven to be an effective tool in smart farming, including plant phenotyping (Mishra et al., 2020), and monitoring crop yield and nutritional status (Sishodia et al., 2020), suggesting its potential for microalgae biofilms in process monitoring.

Microalgal biofilms and plant leaves share several traits, such as pigment signatures and a complex 3D cell organization into layers (Fanesi et al., 2019), which results in similar reflectance patterns. Given their analogous architectural organization and structure, we hypothesized that reflectance indices (RIs) typically utilized to estimate vegetation characteristics in higher plants, might be adapted for monitoring microalgal biofilm systems.

Reflectance technology (hyperspectral/RGB cameras and reflectance spectroscopy) has been employed to monitor natural biofilm assemblages but, to the best of our knowledge, it has never been tested on microalgal biofilms developed for biotechnological purposes. Under process conditions, biomass and compounds reach higher areal densities than those recorded for natural communities (Launeau et al., 2018), and new RIs must be developed to predict target molecules of interest. For instance, the light behavior within the complex 3D structure of biofilms and the presence of extracellular polymeric substances may hinder the utilization of the classical RIs (Decho et al., 2003). Therefore, developing a monitoring protocol that is effective across various biofilm traits and validated regardless of the growing conditions (nutrients, light, and maturation stage) is crucial for the reliable monitoring and control of biofilm-based processes.

This study aims to demonstrate how reflectance spectroscopy and RIs can non-invasively monitor a wide dynamic range of biomass and pigment content in *Haematococcus pluvialis* within a rotating biofilm-based system. *H. pluvialis* was selected as the experimental organism due to its significant changes in pigments, structure and composition throughout its complex life cycle, specifically during astaxanthin production (Shah et al., 2016).

2. Materials and methods

2.1. Experimental setup and biofilm traits

All cultivation protocols for planktonic cultures and biofilm cultivation in the rotating system are detailed in Morgado et al. (2023). Briefly, planktonic cultures of *Haematococcus pluvialis* CCAC 0125 from the Central Collection of Algal Cultures (CCAC) at the University of Duisburg-Essen (UDE), Cologne, Germany, were grown in two batch reactors (2-L each) for 7 days and used as the inoculum for the rotating biofilm system. This system consisted of four rotating cylinders where cotton carriers were employed for biofilm growth, allowing for the monitoring and modulation of pH, light, and nutrient conditions over time.

The effect of several growth conditions was explored by employing a two-stage cultivation strategy over 15 days. Initially, all four reactors were maintained under nitrogen-replete (N-replete) conditions for 7 days (so-called green stage) and exposed to two different photosynthetic photon flux densities (PPFDs): two reactors were maintained at 50 μmol m^{-2} s^{-1} and the other two at 200 μmol m^{-2} s^{-1}. Subsequently, the PPFD was increased to either 400 or 800 μmol m^{-2} s^{-1}, and the nitrogen regime was changed. To induce the red stage, two of the reactors were switched to N-deplete conditions, while the remaining were maintained under N-replete conditions. The biofilm traits of interest were biomass, astaxanthin and chlorophyll areal densities (g m^{-2}) and astaxanthin and chlorophyll content (as a percentage of dry weight, % DW). To characterize these traits over time, sampling was conducted at consistent intervals of time during the 15-day experiment, beginning on day 0 (4 h after inoculation). At each time point, a cotton carrier from each reactor was harvested, and the biofilms were re-suspended for dry weight estimation and pigment (chlorophyll *a* and *b*, and astaxanthin) quantification. The data about biofilm traits (i.e. dry weight and pigments) reported and utilized in this study were sourced from Morgado et al. (2023) (see summary in Table 1).

2.2. Reflectance spectroscopy

The overall pipeline of analysis developed to select predictive models for the monitoring of microalgae biofilm traits is reported in Fig. 1.

To investigate the relationships between reflectance spectra and biofilm traits, the cotton carriers with the biofilms were first scanned using a spectrometer (FLAME-S-VIS-NIR-ES, Ocean Insights), equipped with a 400-μm diameter fiber optic (QR400-7-VIS-NIR, Ocean Insights) and a 20 W tungsten halogen light source (HL-2000-FHSA, Ocean Insights). The halogen lamp was warmed up for at least 15 min before

Table 1
Ranges of selected biological traits investigated for *H. pluvialis* biofilm (number of samples $n = 174$).

Biofilm traits	Unit	Min	Max	Range
Biomass Areal Density	g m^{-2}	2.45	72.66	70.21
Astaxanthin Density	g m^{-2}	0.002	1.713	1.711
Astaxanthin Content	% DW	0.1	4.0	3.9
Total Chlorophyll Content	% DW	0.4	2.3	1.9
Chlorophyll Density	g m^{-2}	0.04	1.01	0.97

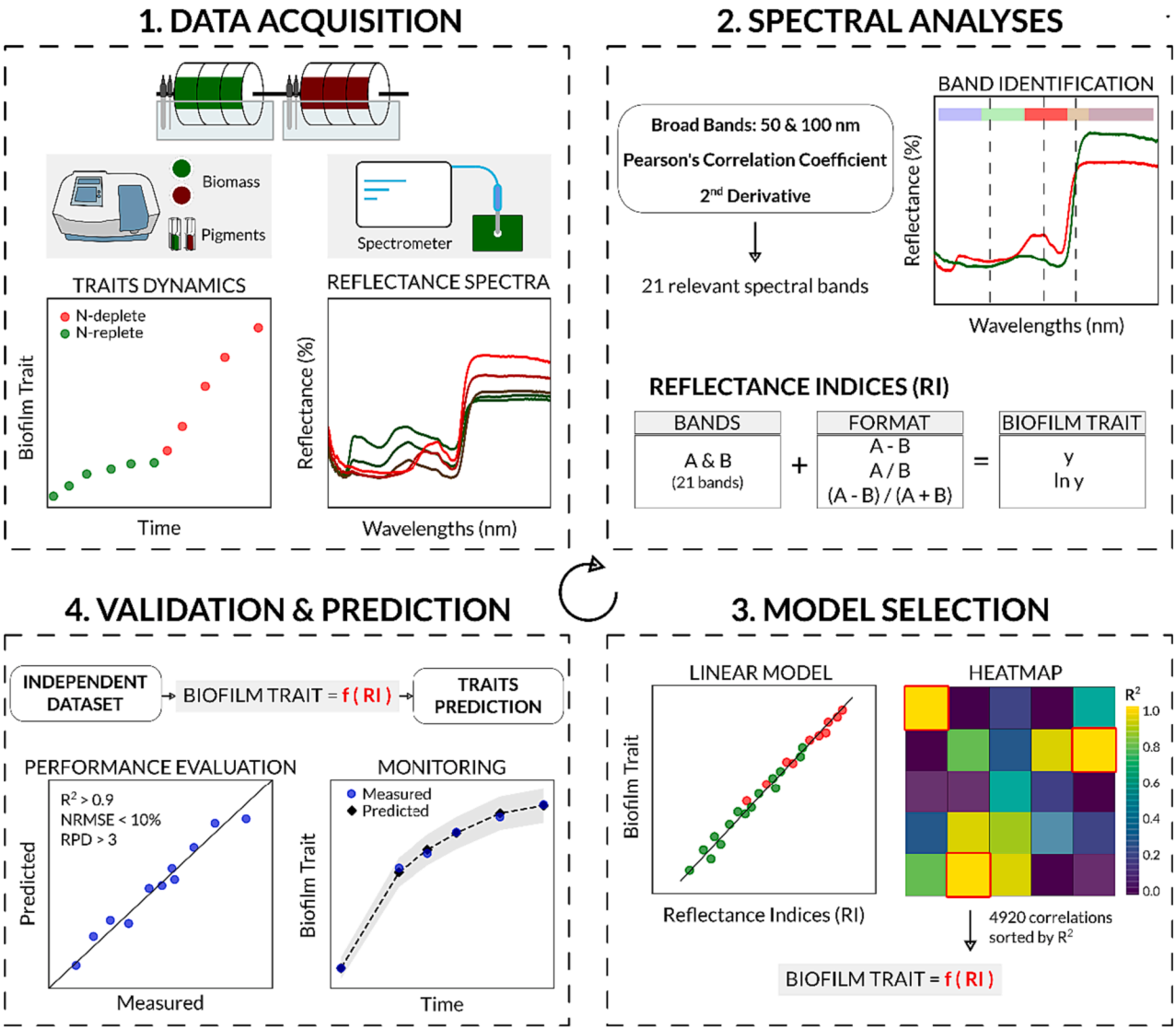

Fig. 1. Workflow depicting the protocol utilized to develop and evaluate the regression models based on reflectance spectra. Initially, biofilm traits were quantified in parallel with the acquisition of reflectance spectra (1). Next, spectral analyses were conducted to identify relevant bands (A and B) and construct reflectance indices (2). These indices were then utilized to develop and calibrate linear models, selecting the best indices for each biofilm trait (3). Subsequently, the models were validated on an independent dataset to evaluate their predictive performances (4).

starting the measurements, and the reflectance probe was fixed to a stand to have the tip of the sensor at 1 cm and at 90 degrees from the biofilm, corresponding to an approximate measured area of 0.5 cm^2. Before the measurements, a white reference corresponding to 100 % reflectance was recorded (WS-1-SL Spectralon Reflectance Standard, Ocean Insights) and the dark current noise subtracted. The spectra were measured from 350 to 1000 nm. For the acquisition of each spectrum, the following parameters were set in OceanView 2.0 (Ocean Insights) spectroscopy software: integration time of 30 ms, 20 accumulations, and a boxcar width of 5. For each sample (biofilm on cotton), 18 positions were measured covering the whole surface of the biofilm. The resulting spectra from each cotton carrier were averaged to obtain one representative spectrum for each sampling day (see supplementary material).

2.3. Spectral bands and indices selection

Reflectance indices (RIs) are calculated using the reflectance in the visible (blue, green, red and red edge regions; 400–700 nm) and in the near-infrared (NIR; 700–1000 nm) spectral regions. To identify the most appropriate RIs for monitoring biomass and pigments in *H. pluvialis* biofilms, the spectral bands most closely correlated with these biofilm traits were identified by dissecting the reflectance spectra into broad and narrow bands.

In the broad bands approach, the spectra were partitioned into multiple bands from the visible to the NIR ranges, specifically in ranges of 100 and 50 nm bandwidth (the specific ranges are reported in Table 2). Subsequently, the spectra of *H. pluvialis* were closely examined to select specific wavelengths. This was achieved by computing Pearson's correlation coefficient between wavelengths and each response variable (biofilm traits). Additionally, the second derivative of the spectra was calculated using the Savitzky–Golay filter, amplifying spectral inflections and enhancing the detection of small spectral variations.

Several RIs have been proposed and used in the literature (see Sishodia et al., 2020; Xue & Su, 2017). Employing a method previously used by Atzberger et al. (2015), all possible two-pairs combinations of the selected spectral bands were computed to determine the best RIs. This approach utilizes the most common RIs formats: Difference Index (*D-Index*), represented by A-B; Ratio Index (*R-index*), represented by A/B; and Normalized Difference Index (*ND-Index*), represented by (A-B)/

Table 2
All A- and B-bands used in the two-pair combinations to compute the reflectance indices.

Vis-NIR spectra	Type	Reflectance Bands*	Wavelengths (nm)
Blue	B	R_{Blue}	400 – 500
		R_{Blue1}	400 – 450
		R_{Blue2}	450 – 500
Green	B	R_{Green}	500 – 600
		R_{Green1}	500 – 550
		R_{525}	522 – 528
		R_{Green2}	550 – 600
		R_{563}	560 – 566
Red	A and B	R_{Red}	600 – 700
		R_{Red1}	600 – 650
		R_{637}	634 – 640
		R_{Red2}	650 – 700
		R_{678}	675 – 681
Red-Edge	A	$R_{Red\ Edge}$	700 – 800
		$R_{Red\ Edge1}$	700 – 750
		R_{715}	712 – 718
		$R_{Red\ Edge2}$	750 – 800
NIR	A	R_{NIR}	750 – 900
		R_{NIR1}	800 – 900
		R_{NIR2}	800 – 850
		R_{NIR3}	850 – 900

*R: Reflectance band used in the reflectance index.

(A + B), where A and B are specific bands of the reflectance spectra (see Table 2). The NDVI (Normalized Difference Vegetation Index; R_{NIR}-R_{Red} / R_{NIR} + R_{Red}, Rouse, 1974), one of the first and still most commonly used RI utilized as an estimate of plant or algae biomass in the literature, was also computed for comparison.

To ensure meaningful and non-inverted correlations, the red (600–700 nm), red-edge (700–800 nm) and NIR (750–900 nm) regions were selected as A-bands, while the blue (400–500 nm), green (500–600 nm), and red (600–700 nm) regions were selected as the B-bands.

2.4. Statistics

All computations were conducted in the R environment 4.3.1 (R Core Team, 2022) and Python 3.9.13. For each index-biofilm trait combination, a linear regression was computed to identify the indices that best fit the biofilm traits, and logarithmic transformations of the traits were also performed to account for non-linear patterns (number of samples n = 174). The goodness of fit for each calibration was assessed using the coefficient of determination, R^2. A heatmap, based on the R^2 values of each regression, was also performed to visualize common behaviors of the RIs as a function of the biofilm traits. Once the calibration with the highest R^2 was identified for each trait, its predictive capabilities were assessed on an independent validation set (n = 22), consisting of additional assays (50, 200 and 400 PPFD with N-replete and N-deplete) performed as described in the experimental setup section. The predictive performance of the linear regressions was based on several metrics, including the R^2, the root square mean error of prediction (RMSEP), the normalized RMSEP (nRMSEP) based on the difference between the maximum and minimum observed measurements, and the residual predictive deviation (RPD). All layouts were generated in Inkscape 1.3 (Harrington et al., 2003).

3. Results and discussion

3.1. Spectral analyses

Reflectance spectroscopy is one of the main remote sensing techniques used in smart agriculture for monitoring plant growth and health, and optimizing production processes (Walsh et al., 2020). The implementation of this monitoring technique could lead to an efficient and "smarter" way of farming microalgae biofilms, which could provide an integrated and holistic approach to agriculture and microalgae production (Lim et al., 2022).

A representative example of spectral dynamics is reported in Fig. 2 for the biofilms grown at 200 μmol m^{-2} s^{-1}, and then subjected to 400 μmol m^{-2} s^{-1} under N-replete and N-deplete conditions. The reflectance signatures of *H. pluvialis* biofilms were strongly impacted by the nutrient and light conditions. The extraction of each reflectance band (see supplementary material) revealed that during early maturation stages of the biofilms, the reflectance in the blue, green, and red regions, decreased (from 20 to 10 %), while the red-edge and NIR remained constant at 30–35 %. From day 7, when the biofilms were N-replete (green stage), the reflectance in the green and blue regions further decreased to 5 %, while the reflectance in the red region decreased to 10 %. The red edge did not remarkably change and the NIR increased over time from 30 to 45 %. Similarly, when the biofilms were N-deplete (red stage), the reflectance in the blue and green also decreased to 5 % and the NIR reached 45 % on day 15. However, there was a clear shift in the red and red-edge bands, which increased from 10 to 15 % and from 30 to 40 %, respectively.

These spectral patterns could be compressed using RI which are efficient parameters that can be used to simplify complex reflectance information (multivariate spectral dataset) for predicting biological traits of photosynthetic organisms (Myneni et al., 1995). Typically, these are calculated as a combination of an absorbing and non-absorbing band (e.g. Vis and NIR, respectively) (Huete, 2012) (referred to here as A- and B-bands). The classical approach for indices formulation relies on the combination of broad spectral ranges (50–100 nm bandwidth) known from the literature (Hennessy et al., 2020). In this study, both classical spectral ranges (blue, green, red, red-edge and NIR regions; 50–100 nm bandwidth) and more specific bands were combined in three RIs formats to describe the traits of *H. pluvialis* biofilms and increase the sensitivity to detect specific compositional changes (Hansen & Schjoerring, 2003).

The selection of specific bands was based on Pearson's correlation coefficient and 2nd derivatives analysis. Fig. 3 shows that the reflectance in the NIR region (750 – 900 nm) was positively correlated with biomass (r = +0.9) and chlorophyll areal density (r = +0.7), while the green region (500 – 600 nm), specifically the wavelength 563 nm, were found to be negatively correlated (r = -0.75). The correlation spectra for chlorophyll and astaxanthin content were mirrored (Fig. 3). These findings align with the literature, where the chlorophyll:carotenoids ratio is a widely used metric for monitoring astaxanthin accumulation and as a stress indicator in microalgae (Solovchenko, 2023). The green region (500 – 600 nm), and in particular the wavelength 563 nm, was positively correlated with chlorophyll (r = +0.5), while negatively correlated with astaxanthin (r = -0.5). The red-edge and NIR regions (700 – 900 nm), and more specifically the wavelength 715 nm, were found to be positively correlated with astaxanthin (r = +0.8) and negatively correlated with chlorophyll (r = -0.8).

The second derivative transformation of the green and red stages spectra also highlighted other interesting bands and inflection points that changed over time (see supplementary material). The wavelengths 420, 525, 637 nm were found to be the most relevant to these changes. Additionally, the wavelength 678 nm was also chosen, a spectral region commonly used in other reflectance studies to represent chlorophyll (Yang et al., 2017). Overall, 21 bands were identified and selected as reflectance A- and B-bands implemented in the RIs to predict *H. pluvialis* biofilm traits (Table 2).

3.2. Reflectance indices

Considering all combinations of 21 bands (164), indices formats (3), and data transformations (ln, non-ln) on five biofilm traits, a total of 4920 linear regressions were performed. A heatmap was generated to provide a comprehensive overview of all combinations and the corresponding R^2 values for each regression model (Fig. 4).

Five calibrations were selected, and the results showed that the *D-*

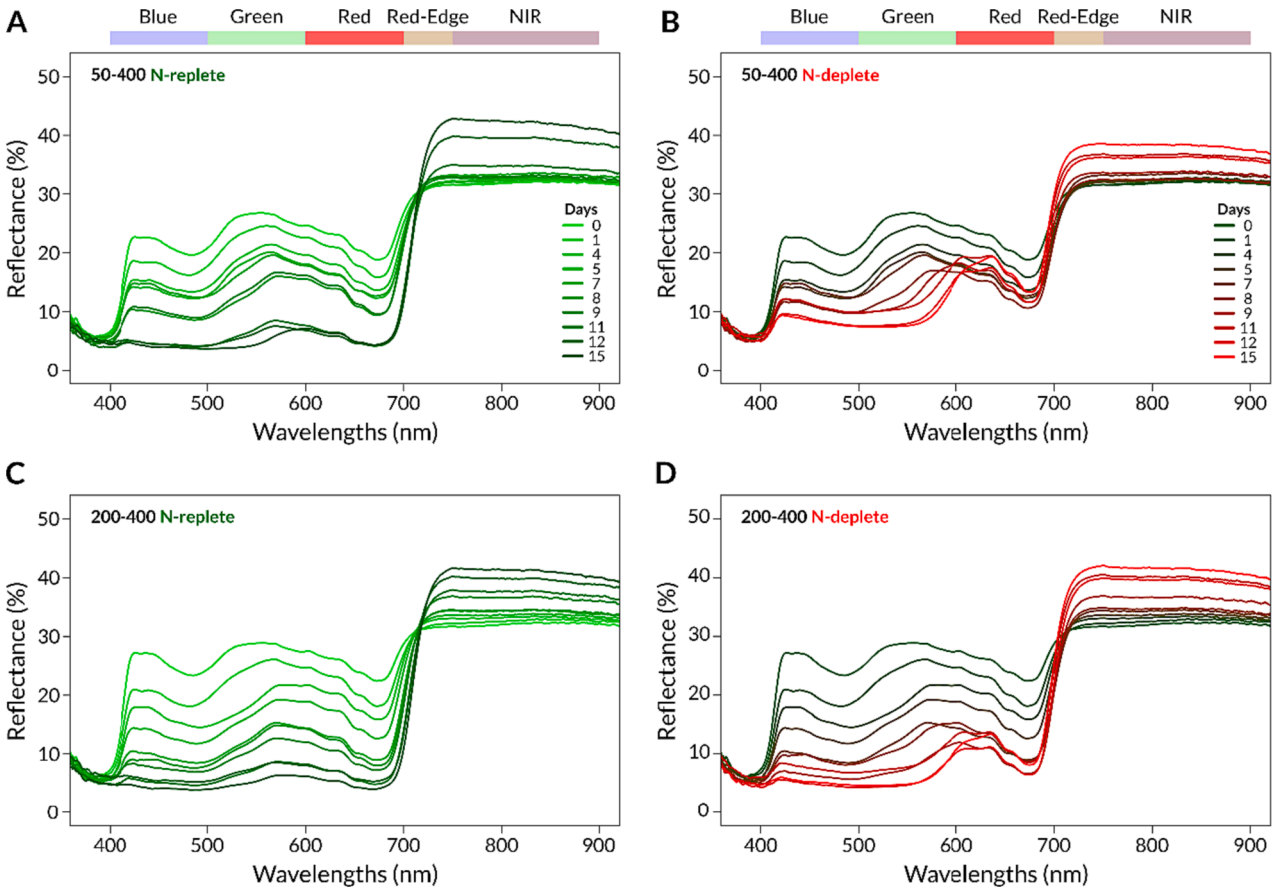

Fig. 2. Representation of the average reflectance spectra over time (from day 0 to day 15) for the biofilm cultivated under 50 and 200 μmol m^{-2} s^{-1} and later (at day 7) subjected to 400 μmol m^{-2} s^{-1} under both N-replete (green) and N-deplete conditions (red). The broad bands used in classical reflectance studies are highlighted. The color gradient used for the spectra has been chosen purely for graphical representation. Other conditions are illustrated in supplementary materials.

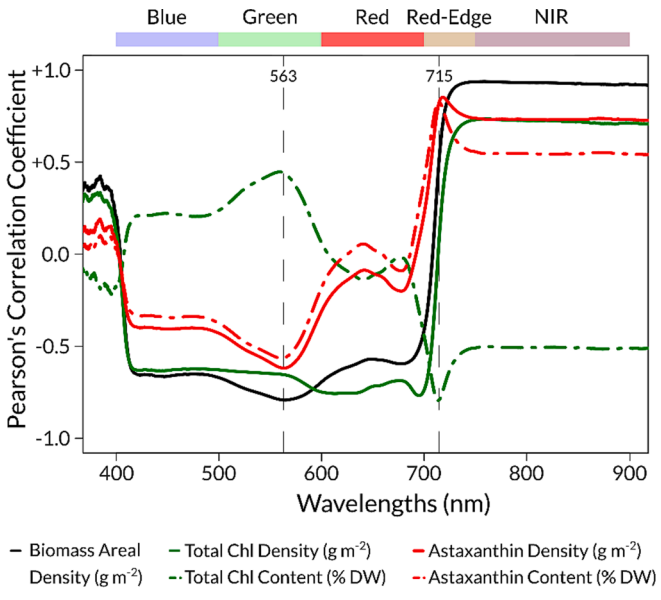

Fig. 3. Correlation spectra based on Pearson's correlation coefficients. Each wavelength of the reflection spectra was correlated to a biofilm trait to generate a specific correlation spectrum. Spectral bands with positive *r* are positively correlated to a trait, whereas bands with negative *r* are negatively correlated. Regions of the spectrum with $r = 0$ do not correlate with the trait.

index was the most effective RI for estimating biomass and astaxanthin areal density (g m^{-2}) as well as astaxanthin content (% DW). The *ND-index* fit, at best, the total chlorophyll content and areal density. While the format of a given RI may help to linearize and/or normalize relationships, the trait-related information encoded by each index is dependent on its spectral bands.

3.2.1. *Trait-specific bands*

Among the 21 bands selected, only 7 were required to precisely capture the dynamic of all biofilm traits. These spectral bands were clearly trait-specific, in agreement with studies on higher plants (Sishodia et al., 2020). Considering the A-band, it can be seen from the heatmap (Fig. 4) that density-related traits such as biomass, astaxanthin and chlorophyll were best described by indices with NIR or red-edge as the reference A-band (see color annotations for the bands). This observation is not surprising, given that the NIR region is not influenced by photosynthetic pigments and might reflect the biomass and possibly the structure (e.g., thickness) of a biofilm. Indeed, NIR sensitivity to the increasing biomass in plants is attributed to an enhanced reflectance due to multiple scattering of light as vegetation layers grow (Ustin & Jacquemoud, 2020). Additionally, from a structural point of view, leaf mesophyll thickness has been reported to positively correlate with NIR reflection (Ollinger, 2011).

On the other hand, total chlorophyll and astaxanthin content (% of DW) was best described by RIs containing A-bands represented by either narrow or broad bands in the red region of the spectra (600–650 nm). Under high-light and N-deplete conditions, astaxanthin accumulation and chlorophyll decrease resulted in a complex reorganization of the spectral signatures of *H. pluvialis* (Morgado et al., 2023), comparable to

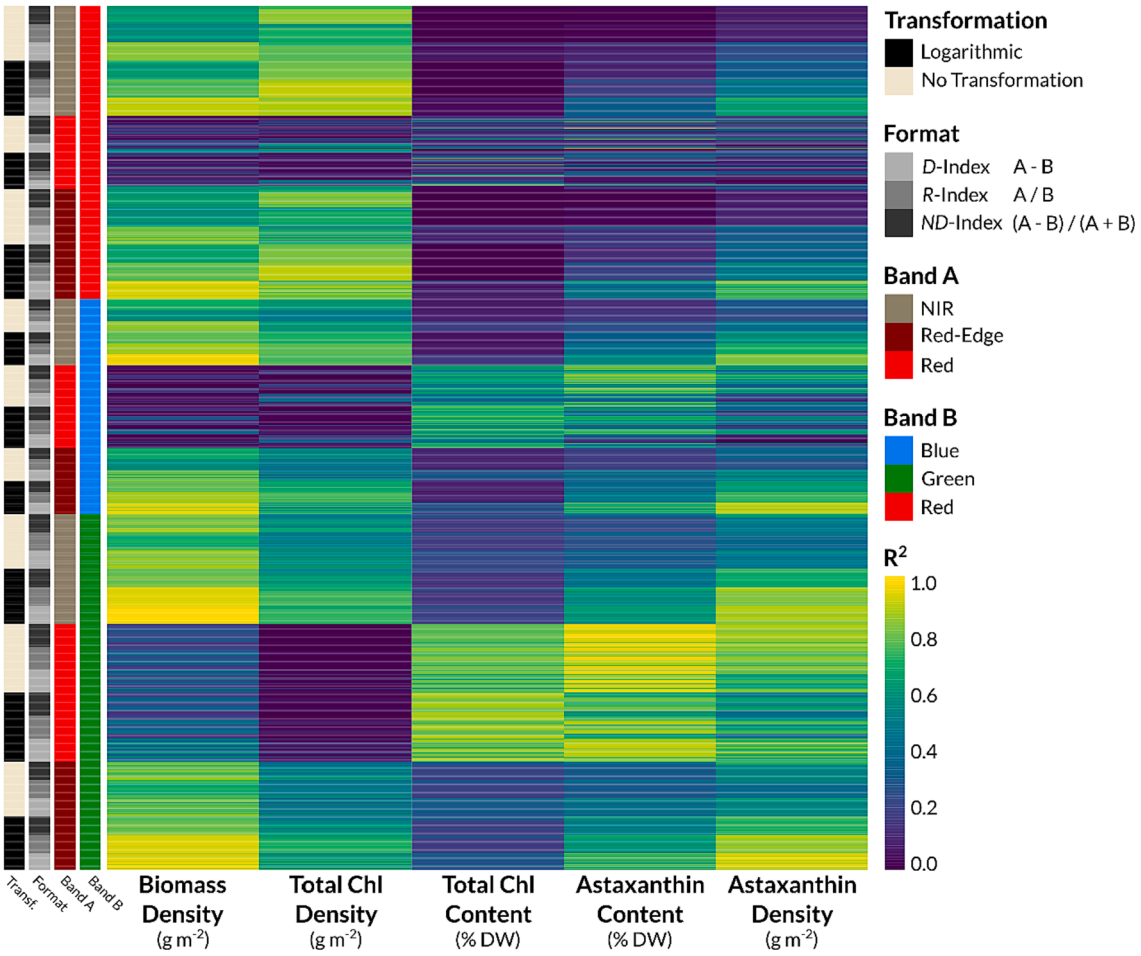

Fig. 4. Heatmap illustrates the correlation coefficients (R2 values) for each linear regression between reflectance indices (RIs) and corresponding biofilm trait. The RIs were obtained from all combinations of 21 selected bands, which include A-bands (Red, Red-Edge, and NIR) and B-bands (Blue, Green, and Red), three equation formats (*D-index*, *R-index*, *ND-index*) and two data transformations (ln, non-ln). On the left, the RIs structure is categorized by data transformation, index format, and band type combination, facilitating the visual identification of the most strongly correlated RI clusters with biofilm traits.

those described for leaves accumulating anthocyanin (a protective carotenoid in higher plants) (Gitelson et al., 2006; Mielke et al., 2012). The accumulation of astaxanthin (absorption peak at around 480 nm) led to a decrease in reflectance in the green, while the loss of chlorophyll contributed to an increase in reflectance in the red and red-edge regions. This caused the formation of a well-defined band at around 637 nm (Fig. 2), which could be used as the reference A-band to accurately describe the trends of pigment content in the biofilms.

Differently from the A-band, the B-band was not trait-specific and, regardless of the trait and index format, was mainly (in four out of five indices) represented by the green region, either in the form of broad (550–600) or narrow band (R_{525}). In microalgae, reflectance in this window is attributed to the "green gap," a region in the electromagnetic spectrum where chlorophylls and carotenoids weakly absorb light, resulting in a consistent amount of reflected light (Schulze et al., 2014). For density-related traits, as the biomass areal density increased, green reflectance consistently decreased until day 15 under both nitrogen conditions and irrespective of the PPFD used (Fig. 2 and supplementary material). This phenomenon may be attributed to changing optical properties of the biofilms as they grow and mature. It is described in higher plants that leaves become optically denser due to a higher packing of pigments per unit area, leading to a greater absorption of light and lower reflectance in the green (Hansen & Schjoerring, 2003). As for the quantification of pigments, the observed decrease in green reflectance is primarily attributed to the increasing accumulation of astaxanthin within the biofilm, aligning with the trends previously discussed.

3.2.2. *Condition-dependent bands*

In this study, the red band was strongly condition-dependent: when the light was increased and the biofilms were N-deplete, they displayed a higher reflectance than that of N-replete biofilms (Fig. 2 and supplementary material). This divergent pattern made classical approaches, such as employing the NDVI index, less successful in describing biomass trends (lower R^2 value) and unable to distinguish those conditions (Fig. 5F). Conversely, the red band was useful in describing the chlorophyll areal density. A decrease in chlorophyll resulted in an increase in reflectance at the red edge, causing a red shift towards the red end of the spectrum. This can be easily observed in the trends of the spectral signatures reported in Fig. 2 and by the 2nd derivate of the spectra (supplementary material). These findings align with previous research suggesting that red-edge based vegetation indices are more effective than NDVI in several areas, such as estimating foliar pigments, providing a more generalized leaf area index (LAI) for different crops, and assessing plant nutrient status (Dong et al., 2019; Gitelson & Solovchenko, 2018).

3.3. *Models prediction performances*

A robust monitoring sensor must be sensitive, able to work under a variety of conditions, and cover a wide dynamic range (Havlik et al., 2022). The five calibrations that were selected, precisely described the

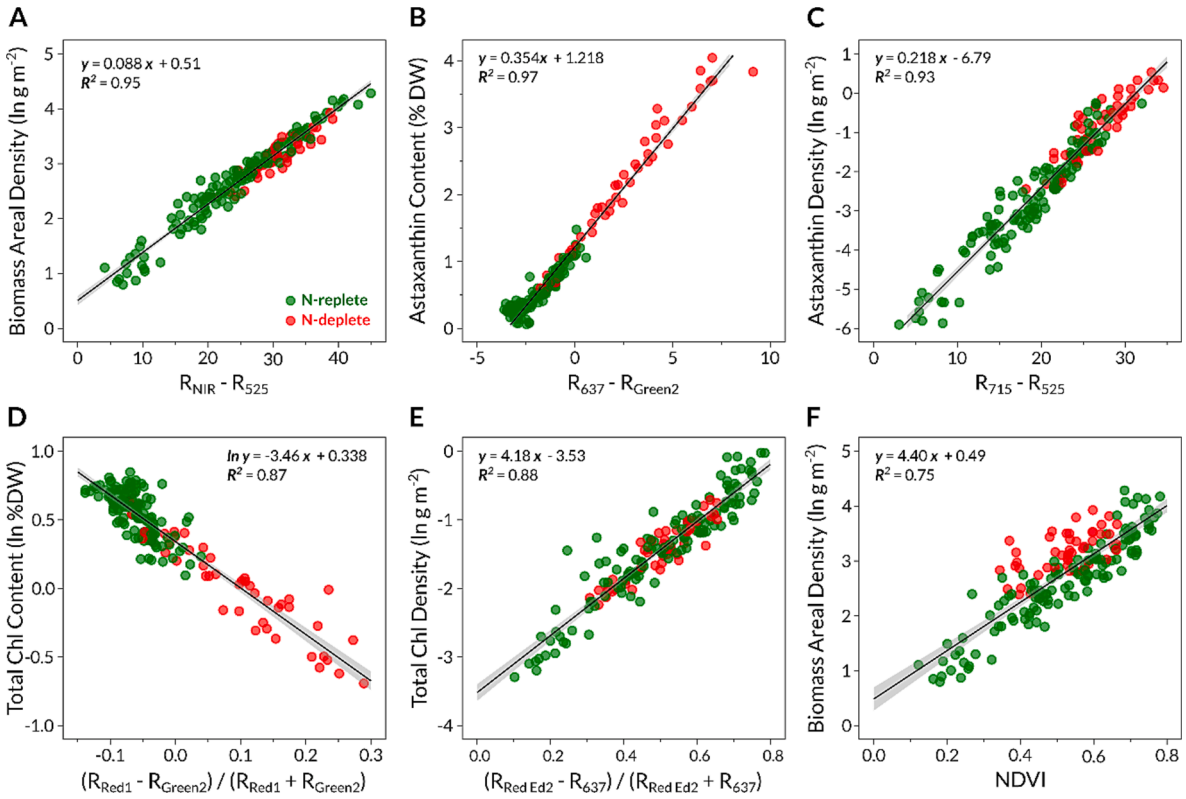

Fig. 5. Regression models computed between the reflectance indices (RIs) and each biofilm trait. A total of 174 biofilm samples grown under different nutrient and light regimes were used for all regressions. Color coding illustrates the samples that were subjected to an N-deplete (red) or an N-replete (green) regime. The equation and respective data transformation, and the R^2 of each regression are also reported. Each panel is dedicated to a particular biofilm trait: (A) biomass areal density; (B) and (C) astaxanthin content and density, respectively; (D) and (E) total chlorophyll content and density, respectively. In panel (F), the NDVI is shown as it is typically the index utilized as an estimate of plant or algae biomass in the literature. This panel is included as a comparison to the predictive model presented in panel (A). The 95% confidence interval is visually represented by the grey area that envelopes the regression model.

relationships between the RIs and the biofilm traits, as suggested by the R^2, which ranged between 0.86 and 0.97 (Fig. 5). Also, the validation of the models on an independent dataset revealed that they were highly accurate in predicting new observations, as indicated by the performance metrics: R^2 values above 0.9, nRMSEP below 10 %, and RPD values above 3 (Alexander et al., 2015; Williams & Sobering, 1993) (Fig. 6, Table 3 and supplementary material).

The sensor demonstrated a very sensitive response to changes in biofilm areal density, detecting microalgae attachment to cotton carriers within just four hours after inoculation (biomass areal density of 3.0 ± 0.5 g m^{-2}). This makes it suitable for the rapid detection of biomass and associated compositional changes due to environmental conditions (linked to nutrient limitation or high light) in the early phases of biofilm development (Li et al., 2024), or in late maturation stages when detachment may occur (Boelee et al., 2011).

By using controlled conditions for microalgae biofilm cultivation and a robust sample size (n = 174), the dynamic ranges for biomass and chlorophyll densities that could be achieved (Table 1) were four times greater than those previously utilized to evaluate reflectance spectroscopy as a remote sensing technique (Launeau et al., 2018). This allowed the sensor to be tested under conditions closer to those encountered in commercial processes, where traits with a wide dynamic range may encounter saturation or non-linearity, particularly when using indices like NDVI (Huang et al., 2021). Data transformation techniques and the use of weights have been successfully implemented for this purpose (Xue & Su, 2017). Here, the natural logarithmic transformation of four traits effectively linearized the relationships between RIs and biofilm traits across their entire dynamic ranges (Fig. 6 and Table 3).

All biofilm trait-RIs relationships could be accurately described using linear regression models with high predictive performances (Table 3), regardless of the conditions considered. The fact that a single model could be built for each biofilm trait suggests good flexibility under several operational conditions (i.e. light, nutrients and maturation stage) making it a perfect candidate for industrial applications.

3.4. *Applications, challenges and future perspectives*

Spectroscopy is a powerful tool for predicting planktonic microalgae traits in biotechnological processes (Podevin et al., 2018). This study represents, to the best of our knowledge, the first in-depth report on the use of RIs for monitoring microalgae biofilms in a process towards biotechnological applications.

Although the reflectance sensor was utilized here to monitor the production of a high-value compound, several other applications can be envisaged. In wastewater treatment, the sensor could be used to track biomass accumulation or observe changes in community composition over time (Paquette et al., 2020). Furthermore, it could be utilized for detecting predators or biological contaminants as part of a quality control strategy (Reichardt et al., 2020). For instance, different microalgae taxa have been already discriminated based on their reflectance spectral fingerprints due to distinct pigment signatures (Solovchenko, 2023).

On the other hand, although the method was found to be robust, three categories of challenges could be identified: biofilm-related, sensor-related and computational.

The calibrations were validated under a controlled set of conditions designed to simulate a two-stage astaxanthin production process. However, to further test the robustness of the sensor, future studies should examine variations in conditions over time, such as repeated harvest and re-growth cycles (Mousavian et al., 2023), and cell recovery

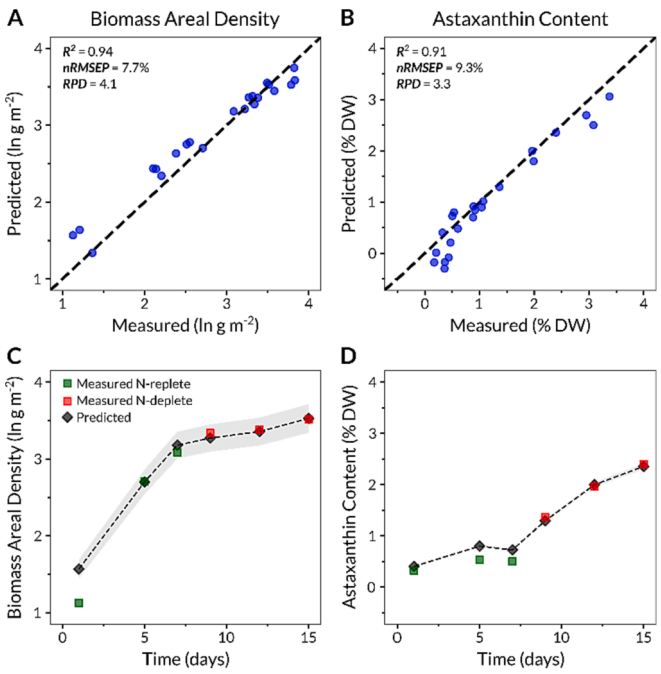

Fig. 6. Comparative analysis of *H. pluvialis* biofilm traits predicted using the regression models identified in this study and quantified with the traditional measurements. The validation step was conducted on independent datasets under the condition of 200 μmol m^{-2} s^{-1} (green stage) and 400 μmol m^{-2} s-1 (red stage). Panels (A) and (B) compare the predicted versus actual measurements, underscoring the models' efficacy through performance metrics such as the coefficient of determination (R^2), normalized root mean square error of prediction (nRMSEP), and residual predictive deviation (RPD). Panels (C) and (D) illustrate the biofilm traits dynamics over time of both predicted and measured trait values. The 95 % confidence prediction interval is visually represented by the grey area that envelopes the predictive data. Panels (A) and (C) represent the biomass areal density, expressed in natural logarithm (ln), while panels (B) and (D) focus on astaxanthin content, expressed as a percentage of dry weight (% DW).

after cessation of the stress (Zhang et al., 2017). Additionally, unforeseen acclimation strategies in biofilms, could introduce bias in the sensor results. Wang et al. (2015) observed a decrease in pigment content as biofilm biomass accumulated. In this scenario, lower pigment levels would result in increased green reflectance, despite an increase in biomass, and a re-computation of bands would be necessary. When transferring this sensor to other microalgal biofilms, some species with higher extracellular polymeric substance excretion could also alter light penetration and scattering, the so-called "biofilm gel effect", thus affecting reflectance patterns (Decho et al., 2003).

A critical consideration of this technology is the unknown depth of penetration of our reference light. In the presence of very thick biofilms, only the top layers may absorb light (Schnurr & Allen, 2015). As a result, the calibrations would reflect only a fraction of the entire community, particularly in samples with a vertical gradient of compounds (Kiperstok et al., 2017). In our study, the maximal biofilm thickness was estimated to be 700–900 μm (data not shown), and a linear response from the sensor was still observed. In the event of thicker biofilms causing a loss of linearity, it would still be possible to increase the penetration depth by using a more powerful light source.

For industrial-scale applications, it is important to consider the spatial resolution of the current sensor. While the present setup is reasonable for homogeneous biofilms, both the measured area (on the scale of cm^2) and spatial resolution might require scaling up to accurately monitor larger biofilm systems. Utilizing alternative sensors already implemented in precision agriculture (Lu et al., 2020) could be advantageous within this context. Moreover, monitoring other biofilm traits and correlating them with operational conditions would help detect technical issues related to evaporation or engine shutdown, which could subject the biofilm to extended periods of stress, such as desiccation. For this purpose, extending the spectrometer configuration to short-wave infrared (SWIR) would broaden the monitoring range of the sensor, encompassing additional physical and compositional properties of the biofilms (García-Sánchez et al., 2017).

Spectral signals are inherently collinear, and linear models may sometimes fail to describe complex spectral-trait relationships. More robust approaches using machine learning techniques may lead to higher predictive performance (Salmi et al., 2022, Ying Ying Tang et al., 2023), providing more precision from a commercial perspective.

Finally, the last challenge lies in the online measurement of biofilm traits, which can be influenced by ambient light, reactor design, and varying biofilm hydration levels, potentially leading to physical alterations in the spectra.

Further research is currently being conducted in our lab to overcome the challenges mentioned above and to optimize the online monitoring of rotating microalgae biofilm-based systems. In particular, the protocol must be tested for other operational factors such as temperature, rotational speed, among others, and extended to other microalgae species, for further validation under a greater variety of conditions likely to be encountered in large-scale applications.

4. Conclusions

This study presents the first protocol for the non-destructive monitoring of microalgae biofilms, establishing reflectance spectroscopy as a viable sensing technique. Our results demonstrate that reflectance indices can reliably reflect microalgae biofilm growth and pigments content, regardless of operational conditions (light, nutrients and maturation stage). This approach provides valuable insights into the development and optimization of microalgae farming, in particular for emerging biofilm-based technologies.

Funding

This project has received funding from the European Union's Horizon 2020 Research and Innovation Program under the Marie Skłodowska-Curie grant agreement No. 955520 DigitAlgaesation.

CRediT authorship contribution statement

David Morgado: Conceptualization, Writing – original draft,

Table 3
Calibration and prediction summary statistics.

Biofilm traits	Calibration			Prediction			
	Index	***Equation***	R^2	R^2	***RMSEP***	***nRMSEP***	***RPD***
Biomass Areal Density (ln g m^{-2})	$R_{NIR} - R_{525}$	y = 0.088 x + 0.51	0.95	0.94	0.21	7.7 %	4.1
Astaxanthin Content (% DW)	$R_{637} - R_{Green2}$	y = 0.354 x + 1.218	0.97	0.91	0.30	9.3 %	3.3
Astaxanthin Density (ln g m^{-2})	$R_{715} - R_{525}$	y = 0.218 x – 6.79	0.93	0.92	0.45	8.2 %	3.7
Total Chlorophyll Content (ln % DW)	$(R_{Red1} - R_{Green2}) / (R_{Red1} + R_{Green2})$	y = – 3.46 x + 0.338	0.87	0.87	0.12	10.8 %	2.8
Total Chlorophyll Density (ln g m^{-2})	$(R_{Red\ Ed2} - R_{637}) / (R_{Red\ Ed2} + R_{637})$	y = 4.18 x – 3.53	0.88	0.81	0.29	11.6 %	2.4

Validation, Formal analysis, Methodology. **Andrea Fanesi:** Writing – original draft, Validation, Methodology, Formal analysis, Conceptualization. **Thierry Martin:** Resources, Conceptualization. **Sihem Tebbani:** Writing – review & editing. **Olivier Bernard:** Writing – review & editing. **Filipa Lopes:** Writing – review & editing, Writing – original draft, Supervision, Resources, Project administration, Funding acquisition.

Declaration of competing interest

The authors declare that they have no known competing financial interests or personal relationships that could have appeared to influence the work reported in this paper.

Data availability

Data will be made available on request.

Acknowledgments

The authors would like also to thank Hélène Santigny for her continuous technical support provided during the experiments. This project has received funding from the European Union's Horizon 2020 Research and Innovation Program under the Marie Skłodowska-Curie grant agreement no. 955520 DigitAlgaesation.

Appendix A. Supplementary data

Supplementary data to this article can be found online at https://doi.org/10.1016/j.biortech.2024.130520.

References

Alexander, D.L.J., Tropsha, A., Winkler, D.A., 2015. Beware of R2: simple, unambiguous assessment of the prediction accuracy of QSAR and QSPR models. J. Chem. Inf. Model. 55 (7), 1316–1322. https://doi.org/10.1021/acs.jcim.5b00206.

Assunção, J., Malcata, F.X., 2020. Enclosed "non-conventional" photobioreactors for microalga production: a review. Algal Res. 52, 102107 https://doi.org/10.1016/j.algal.2020.102107.

Atzberger, C., Darvishzadeh, R., Immitzer, M., Schlerf, M., Skidmore, A., le Maire, G., 2015. Comparative analysis of different retrieval methods for mapping grassland leaf area index using airborne imaging spectroscopy. Int. J. Appl. Earth Obs. Geoinf. 43, 19–31. https://doi.org/10.1016/j.jag.2015.01.009.

Barkia, I., Saari, N., Manning, S.R., 2019. Microalgae for high-value products towards human health and nutrition. Mar. Drugs 17 (5), 304. https://doi.org/10.3390/md17050304.

Blondeau-Patissier, D., Gower, J.F.R., Dekker, A.G., Phinn, S.R., Brando, V.E., 2014. A review of ocean color remote sensing methods and statistical techniques for the detection, mapping and analysis of phytoplankton blooms in coastal and open oceans. Prog. Oceanogr. 123, 123–144. https://doi.org/10.1016/j.pocean.2013.12.008.

Boelee, N.C., Temmink, H., Janssen, M., Buisman, C.J.N., Wijffels, R.H., 2011. Nitrogen and phosphorus removal from municipal wastewater effluent using microalgal biofilms. Water Res. 45 (18), 5925–5933. https://doi.org/10.1016/j.watres.2011.08.044.

Decho, A.W., Kawaguchi, T., Allison, M.A., Louchard, E.M., Reid, R.P., Stephens, F.C., Voss, K.J., Wheatcroft, R.A., Taylor, B.B., 2003. Sediment properties influencing upwelling spectral reflectance signatures: the "biofilm gel effect". Limnol. Oceanogr. 48 (1part2), 431–443. https://doi.org/10.4319/lo.2003.48.1_part_2.0431.

Dong, T., Liu, J., Shang, J., Qian, B., Ma, B., Kovacs, J.M., Walters, D., Jiao, X., Geng, X., Shi, Y., 2019. Assessment of red-edge vegetation indices for crop leaf area index estimation. Remote Sens. Environ. 222, 133–143. https://doi.org/10.1016/j.rse.2018.12.032.

Fanesi, A., Paule, A., Bernard, O., Briandet, R., Lopes, F., 2019. The architecture of monospecific microalgae biofilms. Microorganisms 7 (9), 352. https://doi.org/10.3390/microorganisms7090352.

García-Sánchez, F., Galvez-Sola, L., Martínez-Nicolás, J.J.J.J., Muelas-Domingo, R., Nieves, M 2017. Using Near-Infrared Spectroscopy in Agricultural Systems. In: Developments in Near-Infrared Spectroscopy. IntechOpen. IntechOpen.doi: 10.5772/67236.

Gitelson, A.A., Keydan, G.P., Merzlyak, M.N., 2006. Three-band model for noninvasive estimation of chlorophyll, carotenoids, and anthocyanin contents in higher plant leaves. Geophys. Res. Lett. 33 (11) https://doi.org/10.1029/2006GL026457.

Gitelson, A., Solovchenko, A., 2018. Non-invasive quantification of foliar pigments: possibilities and limitations of reflectance- and absorbance-based approaches. J. Photochem. Photobiol. B: Biol. 178, 537–544. https://doi.org/10.1016/j.jphotobiol.2017.11.023.

Hansen, P.M., Schjoerring, J.K., 2003. Reflectance measurement of canopy biomass and nitrogen status in wheat crops using normalized difference vegetation indices and partial least squares regression. Remote Sens. Environ. 86 (4), 542–553. https://doi.org/10.1016/S0034-4257(03)00131-7.

Harrington, B., Gould, T., & Hursten, N. (2003). Inkscape. https://inkscape.org/.

Havlik, I., Beutel, S., Scheper, T., Reardon, K.F., 2022. On-line monitoring of biological parameters in microalgal bioprocesses using optical methods. Energies 15 (3), Article 3. https://doi.org/10.3390/en15030875.

Hennessy, A., Clarke, K., Lewis, M., 2020. Hyperspectral classification of plants: a review of waveband selection generalisability. Remote Sens. (Basel) 12 (1), Article 1. https://doi.org/10.3390/rs12010113.

Huang, S., Tang, L., Hupy, J.P., Wang, Y., Shao, G., 2021. A commentary review on the use of normalized difference vegetation index (NDVI) in the era of popular remote sensing. J. For. Res. 32 (1), 1–6. https://doi.org/10.1007/s11676-020-01155-1.

Huete, A.R., 2012. Vegetation indices, remote sensing and Forest monitoring. Geogr. Compass 6 (9), 513–532. https://doi.org/10.1111/j.1749-8198.2012.00507.x.

Kiperstok, A.C., Sebestyén, P., Podola, B., Melkonian, M., 2017. Biofilm cultivation of Haematococcus pluvialis enables a highly productive one-phase process for astaxanthin production using high light intensities. Algal Res. 21, 213–222. https://doi.org/10.1016/j.algal.2016.10.025.

Launeau, P., Méléder, V., Verpoorter, C., Barillé, L., Kazemipour-Ricci, F., Giraud, M., Jesus, B., Le Menn, E., 2018. Microphytobenthos biomass and diversity mapping at different spatial scales with a hyperspectral optical model. Remote Sens. (Basel) 10 (5), 716. https://doi.org/10.3390/rs10050716.

Li, S., Fanesi, A., Martin, T., Lopes, F., 2024. Physiological transition of Chlorella vulgaris from planktonic to immobilized conditions. Algal Res. 77, 103354 https://doi.org/10.1016/j.algal.2023.103354.

Lieutaud, C., Assaf, A., Gonçalves, O., Wielgosz-Collin, G., Thouand, G., 2019. Fast non-invasive monitoring of microalgal physiological stage in photobioreactors through raman spectroscopy. Algal Res. 42, 101595 https://doi.org/10.1016/j.algal.2019.101595.

Lim, H.R., Khoo, K.S., Chia, W.Y., Chew, K.W., Ho, S.-H., Show, P.L., 2022. Smart microalgae farming with internet-of-things for sustainable agriculture. Biotechnol. Adv. 57, 107931 https://doi.org/10.1016/j.biotechadv.2022.107931.

Liu, J.-Y., Zeng, L.-H., Ren, Z.-H., 2021. The application of spectroscopy technology in the monitoring of microalgae cells concentration. Appl. Spectrosc. Rev. 56 (3), 171–192. https://doi.org/10.1080/05704928.2020.1763380.

Lu, B., Dao, P.D., Liu, J., He, Y., Shang, J., 2020. Recent advances of hyperspectral imaging technology and applications in agriculture. Remote Sens. (Basel) 12 (16), Article 16. https://doi.org/10.3390/rs12162659.

Mantzorou, A., Ververidis, F., 2019. Microalgal biofilms: a further step over current microalgal cultivation techniques. Sci. Total Environ. 651 (Pt 2), 3187–3201. https://doi.org/10.1016/j.scitotenv.2018.09.355.

Méléder, V., Savelli, R., Barnett, A., Polsenaere, P., Gernez, P., Cugier, P., Lerouxel, A., Le Bris, A., Dupuy, C., Le Fouest, V., Lavaud, J., 2020. Mapping the intertidal microphytobenthos gross primary production part I: coupling multispectral remote sensing and physical modeling. Front. Marine Sci. 7 https://doi.org/10.3389/fmars.2020.00520.

Mielke, M.S., Schaffer, B., Schilling, A.C., 2012. Evaluation of reflectance spectroscopy indices for estimation of chlorophyll content in leaves of a tropical tree species. Photosynthetica 50 (3), 343–352. https://doi.org/10.1007/s11099-012-0038-2.

Mishra, P., Lohumi, S., Ahmad Khan, H., Nordon, A., 2020. Close-range hyperspectral imaging of whole plants for digital phenotyping: recent applications and illumination correction approaches. Comput. Electron. Agric. 178, 105780 https://doi.org/10.1016/j.compag.2020.105780.

Moody, J.W., McGinty, C.M., Quinn, J.C., 2014. Global evaluation of biofuel potential from microalgae. Proc. Natl. Acad. Sci. 111 (23), 8691–8696. https://doi.org/10.1073/pnas.1321652111.

Morales, M., Bonnefond, H., Bernard, O., 2020. Rotating algal biofilm versus planktonic cultivation: LCA perspective. Journal of Cleaner Production 257, 120547. https://doi.org/10.1016/j.jclepro.2020.120547.

Moreno Osorio, J.H., Pollio, A., Frunzo, L., Lens, P.N.L., Esposito, G., 2021. A review of microalgal biofilm technologies: definition, applications, settings and analysis. Front. Chem. Eng. 3 https://doi.org/10.3389/fceng.2021.737710.

Morgado, D., Fanesi, A., Martin, T., Tebbani, S., Bernard, O., Lopes, F., 2023. Exploring the dynamics of astaxanthin production in Haematococcus pluvialis biofilms using a rotating biofilm-based system. Biotechnol. Bioeng. 1–14 https://doi.org/10.1002/bit.28624.

Mousavian, Z., Safavi, M., Salehirad, A., Azizmohseni, F., Hadizadeh, M., Mirdamadi, S., 2023. Improving biomass and carbohydrate production of microalgae in the rotating cultivation system on natural carriers. AMB Express 13 (1), 39. https://doi.org/10.1186/s13568-023-01548-5.

Myneni, R.B., Hall, F.G., Sellers, P.J., Marshak, A.L., 1995. The interpretation of spectral vegetation indexes. IEEE Trans. Geosci. Remote Sens. 33 (2), 481–486. https://doi.org/10.1109/TGRS.1995.8746029.

Ollinger, S.V., 2011. Sources of variability in canopy reflectance and the convergent properties of plants. New Phytol. 189 (2), 375–394. https://doi.org/10.1111/j.1469-8137.2010.03536.x.

Paquette, A.J., Sharp, C.E., Schnurr, P.J., Allen, D.G., Short, S.M., Espie, G.S., 2020. Dynamic changes in community composition of scenedesmus-seeded artificial, engineered microalgal biofilms. Algal Res. 46, 101805 https://doi.org/10.1016/j.algal.2020.101805.

Podevin, M., Fotidis, I.A., Angelidaki, I., 2018. Microalgal process-monitoring based on high-selectivity spectroscopy tools: status and future perspectives. Crit. Rev. Biotechnol. 38 (5), 704–718. https://doi.org/10.1080/07388551.2017.1398132.

Podola, B., Li, T., Melkonian, M., 2017. Porous substrate bioreactors: a paradigm shift in microalgal biotechnology? Trends Biotechnol. 35 (2), 121–132. https://doi.org/10.1016/j.tibtech.2016.06.004.

R Core Team. (2022). R: A Language and Environment for Statistical Computing. R Foundation for Statistical Computing. https://www.R-project.org/.

Reichardt, T.A., Maes, D., Jensen, T.J., Dempster, T.A., McGowen, J.A., Poorey, K., Curtis, D.J., Lane, T.W., Timlin, J.A., 2020. Spectroradiometric detection of competitor diatoms and the grazer poteriochromonas in algal cultures. Algal Res. 51, 102020 https://doi.org/10.1016/j.algal.2020.102020.

Rouse, J. W. (1974). Monitoring the vernal advancement and retrogradation (green wave effect) of natural vegetation (NASA-CR-139243). https://ntrs.nasa.gov/citations/19740022555.

Sá, M., Ferrer-Ledo, N., Gao, F., Bertinetto, C.G., Jansen, J., Crespo, J.G., Wijffels, R.H., Barbosa, M., Galinha, C.F., 2022. Perspectives of fluorescence spectroscopy for online monitoring in microalgae industry. J. Microbial. Biotechnol. 15 (6), 1824–1838. https://doi.org/10.1111/1751-7915.14013.

Salmi, P., Calderini, M., Pääkkönen, S., Taipale, S., Pölönen, I., 2022. Assessment of microalgae species, biomass, and distribution from spectral images using a convolution neural network. J. Appl. Phycol. 34 (3), 1565–1575. https://doi.org/10.1007/s10811-022-02735-w.

Schnurr, P.J., Allen, D.G., 2015. Factors affecting algae biofilm growth and lipid production: a review. Renew. Sustain. Energy Rev. 52, 418–429. https://doi.org/10.1016/j.rser.2015.07.090.

Schulze, P.S.C., Barreira, L.A., Pereira, H.G.C., Perales, J.A., Varela, J.C.S., 2014. Light emitting diodes (LEDs) applied to microalgal production. Trends Biotechnol. 32 (8), 422–430. https://doi.org/10.1016/j.tibtech.2014.06.001.

Shah, Md. M. R., Liang, Y., Cheng, J. J., & Daroch, M. (2016). Astaxanthin-producing green microalga haematococcus pluvialis: from single cell to high value commercial products. Frontiers in Plant Science, 7. https://www.frontiersin.org/articles/10.3389/fpls.2016.00531.

Sishodia, R.P., Ray, R.L., Singh, S.K., 2020. Applications of remote sensing in precision agriculture: a review. Remote Sensing 12 (19), 19. https://doi.org/10.3390/rs12193136.

Slegers, P.M., Olivieri, G., Breitmayer, E., Sijtsma, L., Eppink, M.H.M., Wijffels, R.H., Reith, J.H., 2020. Design of Value Chains for microalgal biorefinery at industrial scale: process integration and techno-economic analysis. Front. Bioeng. Biotechnol. 8 https://doi.org/10.3389/fbioe.2020.550758.

Solovchenko, A., 2023. Seeing good and bad: optical sensing of microalgal culture condition. Algal Res. 71, 103071 https://doi.org/10.1016/j.algal.2023.103071.

Ying Ying Tang, D., Wayne Chew, K., Ting, H.-Y., Sia, Y.-H., Gentili, F. G., Park, Y.-K., Banat, F., Culaba, A. B., Ma, Z., & Loke Show, P. (2023). Application of regression and artificial neural network analysis of Red-Green-Blue image components in prediction of chlorophyll content in microalgae. Bioresource Technology, 370, 128503. https://doi.org/10.1016/j.biortech.2022.128503.

Ustin, S.L., Jacquemoud, S., 2020. How the optical properties of leaves modify the absorption and scattering of energy and enhance leaf functionality. In: Cavender-Bares, J., Gamon, J.A., Townsend, P.A. (Eds.), Remote Sensing of Plant Biodiversity. Springer International Publishing, pp. 349–384. https://doi.org/10.1007/978-3-030-33157-3_14.

Walsh, K.B., Blasco, J., Zude-Sasse, M., Sun, X., 2020. Visible-NIR 'point' spectroscopy in postharvest fruit and vegetable assessment: the science behind three decades of commercial use. Postharvest Biol. Technol. 168, 111246 https://doi.org/10.1016/j.postharvbio.2020.111246.

Wang, J., Liu, J., Liu, T., 2015. The difference in effective light penetration may explain the superiority in photosynthetic efficiency of attached cultivation over the conventional open pond for microalgae. Biotechnol. Biofuels 8 (1), 49. https://doi.org/10.1186/s13068-015-0240-0.

Williams, P.C., Sobering, D.C., 1993. Comparison of commercial near infrared transmittance and reflectance instruments for analysis of whole grains and seeds. J. Near Infrared Spectrosc. 1 (1), 25–32.

Xue, J., Su, B., 2017. Significant remote sensing vegetation indices: a review of developments and applications. Journal of Sensors 2017, e1353691. https://doi.org/10.1155/2017/1353691.

Yang, Z., Reiter, M., Munyei, N., 2017. Estimation of chlorophyll-a concentrations in diverse water bodies using ratio-based NIR/RED indices. Remote Sens. Appl.: Soc. Environ. 6, 52–58. https://doi.org/10.1016/j.rsase.2017.04.004.

Zhang, C., Liu, J., Zhang, L., 2017. Cell cycles and proliferation patterns in Haematococcus pluvialis. Chin. J. Oceanol. Limnol. 35 (5), 1205–1211. https://doi.org/10.1007/s00343-017-6103-8.